



# Predicting electroporation of cells in an inhomogeneous electric field based on mathematical modeling and experimental CHO-cell permeabilization to propidium iodide determination



Janja Dermol, Damijan Miklavčič \*

University of Ljubljana, Faculty of Electrical Engineering, Tržaška 25, SI-1000, Ljubljana, Slovenia

## ARTICLE INFO

### Article history:

Received 17 July 2013

Received in revised form 13 March 2014

Accepted 24 March 2014

Available online 29 March 2014

### Keywords:

Electroporation  
Mathematical modeling  
Propidium iodide  
Cell density  
CHO cells  
Electric field distribution

## ABSTRACT

High voltage electric pulses cause electroporation of the cell membrane. Consequently, flow of the molecules across the membrane increases. In our study we investigated possibility to predict the percentage of the electroporated cells in an inhomogeneous electric field on the basis of the experimental results obtained when cells were exposed to a homogeneous electric field. We compared and evaluated different mathematical models previously suggested by other authors for interpolation of the results (symmetric sigmoid, asymmetric sigmoid, hyperbolic tangent and Gompertz curve). We investigated the density of the cells and observed that it has the most significant effect on the electroporation of the cells while all four of the mathematical models yielded similar results. We were able to predict electroporation of cells exposed to an inhomogeneous electric field based on mathematical modeling and using mathematical formulations of electroporation probability obtained experimentally using exposure to the homogeneous field of the same density of cells. Models describing cell electroporation probability can be useful for development and presentation of treatment planning for electrochemotherapy and non-thermal irreversible electroporation.

© 2014 Elsevier B.V. All rights reserved.

## 1. Introduction

High voltage electric pulses affect membrane's selective permeability. According to the theory electroporation of the membrane occurs as pores are formed in the membrane. Cell membrane thus becomes permeable for different molecules which otherwise cannot pass through the membrane in or out of the cell [1–3]. Increased membrane permeability occurs in the regions of the membrane where the transmembrane voltage exceeds a certain threshold, which is characteristic of each cell line, but also depends on pulse parameters [4,5]. If the cell is able to recover after the exposure to electric pulses we call this reversible electroporation. If the cell cannot recover and it does not survive electroporation we call it irreversible [6]. Electroporation is widely used in different areas—gene transfer [7–9], cancer treatment [10–12], biotechnology [13,14] and food processing [15–17].

When predicting the electroporation of cells, for example in a tissue, it is usually (implicitly) assumed that cells are electroporated if the induced transmembrane voltage exceeds the characteristic threshold [18,19]. If the induced transmembrane voltage is below the characteristic threshold the cells are not electroporated. In reality the transition from non-electroporated to reversibly and irreversibly electroporated

state is continuous. So far different mathematical models of electroporation have been proposed in the literature [20–22]. With the appropriately chosen mathematical model we could predict percentage of cells affected if a certain voltage is applied using specific electrode geometry.

In recent years electroporation based treatments have paved their way to clinical use. Electrochemotherapy for solid cutaneous, subcutaneous tumors and metastasis [11,23], as well as for deep seated tumors [24,25] is being used in clinics. Minimally invasive non-thermal irreversible electroporation as soft tissue ablation has also been proposed [6] and used in animal [26] and human clinics [27]. In all these cases treating deep seated tumors or soft tissue using minimally invasive procedures a need for pretreatment planning was clearly established [28–30]. Until now visualization of electric field distribution is used as being the most important predictor of tissue permeabilization and ablation [25,29,31,32].

There is a considerable number of studies of electroporation in dense cell suspensions available [33–36], but there are much less studies available on tissues [37–39]. In these latter studies besides the density of the cells, applied electric field, cell line, and cells' mutual electric shielding, the connections between the cells and their irregular shape could play an important role as well [4]. In our present study the experiments were performed on monolayers of cells of different densities.

When defining the duration and the voltage of the applied pulses we model the geometry of the electrodes and of the cells as a bulk 2D “tissue” layer. Electric field ( $E$  field) distribution is numerically calculated and

\* Corresponding author. Tel.: +386 1 4768 456.  
E-mail address: [damijan.miklavcic@fe.uni-lj.si](mailto:damijan.miklavcic@fe.uni-lj.si) (D. Miklavčič).

adequate voltage is determined [40]. Because of the complexity of the tissues and electrodes analytical calculations are usually in most cases not possible. There is no conventional or easy way to measure  $E$  field in vivo. We have recently proposed a method based on current density imaging (CDI) and magnetic resonance electrical impedance tomography (MREIT) to measure  $E$  field in biological tissues [41,42]. However, the most reliable or even easy way is numerical modeling which we employed.

Until now, the calculated electric field is thresholded with two different thresholds to obtain three areas—the area where irreversible electroporation occurs, the area where reversible electroporation occurs and the area where electroporation does not occur. The cell response can be approximated with a step function. Electroporation is 100% if the applied electric field is above the characteristic electroporation threshold and 0% if it is below. In the same way area where irreversible electroporation occurs can be modeled. Irreversible electroporation is 100% if the applied electric field is above the characteristic threshold for irreversible electroporation and 0% if it is below.

The aim of our study was to predict a percentage of electroporated cells grown as a dense monolayer exposed to an inhomogeneous field. We performed experiments in a homogeneous electric field and determined the percentage of cell electroporation for a certain applied  $E$ . We used these results in four different mathematical models, which interpolated and extrapolated the percentage of electroporated cells to other values of  $E$ . We used homogeneous  $E$  for calculating parameters of the mathematical models because it is possible to determine the percentage of electroporated cells at a certain  $E$ . We validated the mathematical models by exposing cells to the inhomogeneous field and comparing predicted and experimentally determined values of percentage of electroporation. We used the inhomogeneous electric field for validation because in tumors and tissues the electric field around the electrodes is in almost all cases inhomogeneous. The predicted values were obtained by using the numerically calculated inhomogeneous  $E$  in mathematical models. We obtained the percentage of electroporation in the dependence on  $E$  for the area around the electrodes.

The advantage of this approach is that simple electrode geometry configurations can be used to calculate the parameters of the mathematical models. Mathematical models predicting cell electroporation can then be applied to arbitrary electrode geometry. This kind of mathematical relationship could allow us to present treatment plans in a clearer and more understandable way. At the moment, the treatment plans present the  $E$  field applied to a certain area of a tissue/tumor. Using this method the percentage of the electroporated area of a tissue/tumor could be shown. Eventually also the number and duration of pulses could be taken into account [43].

The block scheme on Fig. 1 shows the procedure used in our study. First, we exposed cells to the homogeneous field (block 1). Based on these results we determined the parameters of a mathematical model of cell electroporation (block 2). We used this mathematical model and inhomogeneous  $E$  field distribution to predict the percentage of electroporation (block 3). We then validated the model by exposing cells to the inhomogeneous field (block 4) by comparing predicted

and experimental values. If the results were not in good agreement, we adjusted the mathematical model (block 2) and repeated the prediction of electroporation and the validation of the mathematical model.

## 2. Methods

### 2.1. Cell line and cell culture

A series of experiments were performed on Chinese hamster ovary cells (CHO). Cells were grown in monolayers of different densities in Petri dishes 40 mm in diameter (TPP, Switzerland) in 2 mL of culture medium (Ham's Nutrient Mixtures HAM-F12, Sigma-Aldrich, Steinheim, Germany) supplemented with 10% FBS, antibiotics and L-glutamine for 2 days at 37 °C and 5% CO<sub>2</sub> (Kambič, Slovenia).

### 2.2. Pulse generator and pulse exposure

For the experiments electric pulse generator Cliniporator (IGEA, Italy) was used. For each experiment one rectangular pulse in the duration of 1 ms was applied. The voltages were chosen so that the maximal electric field in the homogeneous field was 1.6 kV/cm and in the inhomogeneous field it was 2.3 kV/cm. Therefore, for the homogeneous field the applied voltages were between 200 V and 800 V with a step of 200 V while for the inhomogeneous field the applied voltages were between 80 V and 140 V with a step of 20 V. Two different electrode configurations were used. For the homogeneous field two parallel Pt/Ir wire electrodes with 0.75 mm diameter and distance between the inner edges of the electrodes set at 5 mm [44] were positioned at the bottom of the Petri dish (Fig. 2a). For the inhomogeneous field we used one needle electrode pair with diameter 0.5 mm and distance between the inner edges of the electrodes set at 1.0 mm (Fig. 2b) [45].

Cells were exposed to the electric pulses in a medium of 1 mL HAM-F12 and 100  $\mu$ L of 1.5 mM propidium iodide (PI). PI is a non-permeant fluorescent dye, which emits strong fluorescence after entering the cell and thus allows easy determination of cell electroporation and discrimination between electroporated and non-electroporated cells by thresholding fluorescent images (see 2.3 Fluorescence microscopy). After the exposure to an electric pulse the cells were incubated for 5 min at room temperature and then washed with HAM-F12.

### 2.3. Fluorescence microscopy

The cells were observed by an inverted microscope AxioVert 200 (Zeiss, Germany) under 10 $\times$  magnification. In each experiment in the homogeneous field up to five phase contrast and five corresponding fluorescent images were acquired from randomly selected fields of view between the electrodes. In the experiments in the inhomogeneous field four images were acquired when 80 V was applied and nine images when more than 80 V was applied to obtain the area around the electrodes. The number of experiments and images acquired in each experiment for each  $E$  for homogeneous field is shown in Table 1. The number

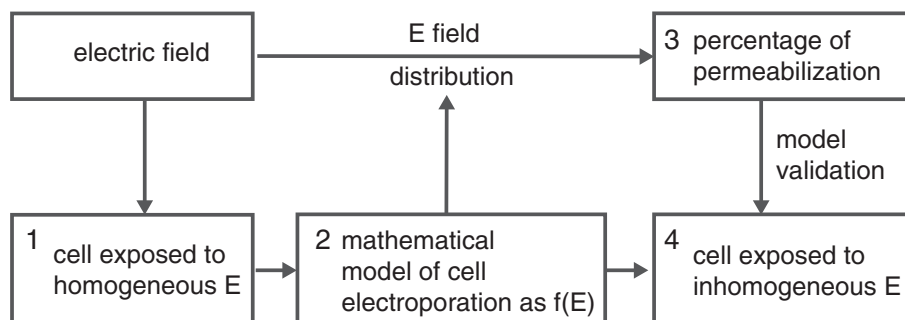
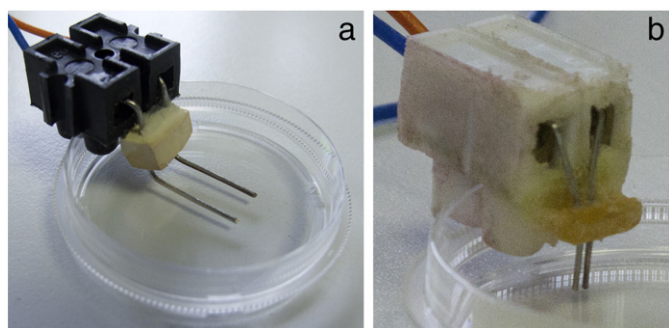


Fig. 1. A block scheme showing the layout of the article. Numbers in the blocks show the temporal sequence of our study.



**Fig. 2.** Photos of electrodes, used in the experiments. a—Two parallel Pt/Ir wire electrodes with 0.75 mm diameter and distance between their inner edges set at 5 mm. b—One needle Pt/Ir electrode pair with diameter 0.5 mm and distance between the inner edges of the electrodes set at 1.0 mm.

of images used at different cell densities is also reported in Table 1. For the inhomogeneous field the number of experiments is reported in Table 2. In each experiment one pair of composed images was acquired (one fluorescent and one phase-contrast image). Fluorescent and phase-contrast images were then stacked together in Adobe Photoshop CS5 (Adobe Systems Inc., San Jose, CA, USA) to get one image of the whole area around the electrodes (Fig. 3a,b). For acquisition we used the VisiCam 1280 camera (Visitron, Germany) and MetaMorph PC software (Molecular Devices, USA).

#### 2.4. Fitting of the mathematical models

First, the acquired fluorescent images from experiments in the homogeneous electric field were thresholded and electroporated cells were manually counted. Cells in the phase contrast images were manually counted as well. The percentage of the electroporated cells and standard deviation were calculated. The results were classified into three groups on the basis of the density of the cells i.e. on the number of the cells on the phase contrast images. The first group was the images with less than 300 cells, second was the images with density in the range from 300 to 600 cells and the third was the images with more than 600 cells per image. In Fig. 4 we can see how different groups of cell densities look like under the microscope. Fig. 4a shows a typical example of a least dense monolayer (less than 300 cells per image), Fig. 4b shows the typical example of a medium dense cell monolayer (from 300 to 600 cells per image) and Fig. 4c shows the densest monolayer (more than 600 cells per image).

Different mathematical models (symmetric sigmoid (Eq. (1)), asymmetric sigmoid (Eq. (2)), Gompertz curve (Eq. (3)) and hyperbolic tangent (Eq. (4))) suggested previously by other authors [20,46,47] were fitted in Matlab (R2010a, Mathworks, USA) to the experimental data of the percentage of electroporated cells in the homogeneous field using the method of non-linear least squares. We obtained an analytical

**Table 2**

Number of experiments (one petri dish and one composed image for one experiment) in the inhomogeneous field.

Voltage applied (V)	Number of experiments
80	9
100	12
120	6
140	8

expression with optimized parameters for each of the equations (Eqs. (1)–(4)).

$$p(E) = 1 / (1 + \exp(-(E - E_{50\%})/b))^* 100\% \quad (1)$$

$$p(E) = (1 + v^* \exp(-(E - E_{50\%})/b))^{(-1/v)} * 100\% \quad (2)$$

$$p(E) = \exp(-\exp(-(E - E_{50\%})/b)) * 100\% \quad (3)$$

$$p(E) = (1 + \tanh(B^*(E - E_{50\%}))) / 2 * 100\% \quad (4)$$

$E_{50\%}$  represents the electric field at which 50% of the cells are electroporated and  $p$  denotes the percentage of electroporated cells in the dependence of the applied electric field. Parameters  $b$  and  $B$  define the width of the curve, e.g. how quickly the cells go from the non-electroporated state to the electroporated state when the electric field is increasing. Parameter  $v$  defines the slope of the Eq. (2).  $E$  in all four equations means the applied electric field.

#### 2.5. Modeling of the inhomogeneous electric field

Numerical calculations of the distribution of the inhomogeneous electric field were performed in COMSOL Multiphysics (version 3.5, COMSOL, Sweden). The model was made in the AC/DC module. The medium around the electrodes had its electrical conductivity set at 1.0 S/m which is the conductivity of the pulsing buffer. Since the pulse duration (1 ms) was much longer than a typical constant for polarization of the cell membrane (around 1  $\mu$ s) [48] steady-state analysis was made. The calculated distribution of the electric field around the electrodes is shown in Fig. 5a.

The area around the electrodes in the inhomogeneous electric field was divided using contours into subareas where the electric field was within a certain range. An example of these contours is presented in Fig. 5b. When 80 V was applied the area was divided into 4 subareas, when 100 V was applied the area was divided into 5 subareas and when 120 V or 140 V was applied the area was divided into 6 subareas. The minimal electric field still analyzed was 0.30–0.39 kV/cm. The limits of the analyzed ranges of electric field for all of the applied voltages are presented in Table 3. Table 3 shows also the percentage of

**Table 1**  
Number of experiments for each voltage in the applied homogeneous field. In each experiment at least three images were acquired from randomly chosen points of view. Number of image pairs (phase-contrast and fluorescent) for each density of the cells is reported in the 3rd, 4th and 5th columns.

Applied voltage (V)	Number of experiments	Number of images (>600 cells/image)	Number of images (300–600 cells/image)	Number of images (<600 cells/image)
200	6	14	10	5
300	4	4	6	3
400	8	11	8	16
500	9	6	25	20
600	6	10	8	10
700	6	9	7	6
800	8	7	22	7

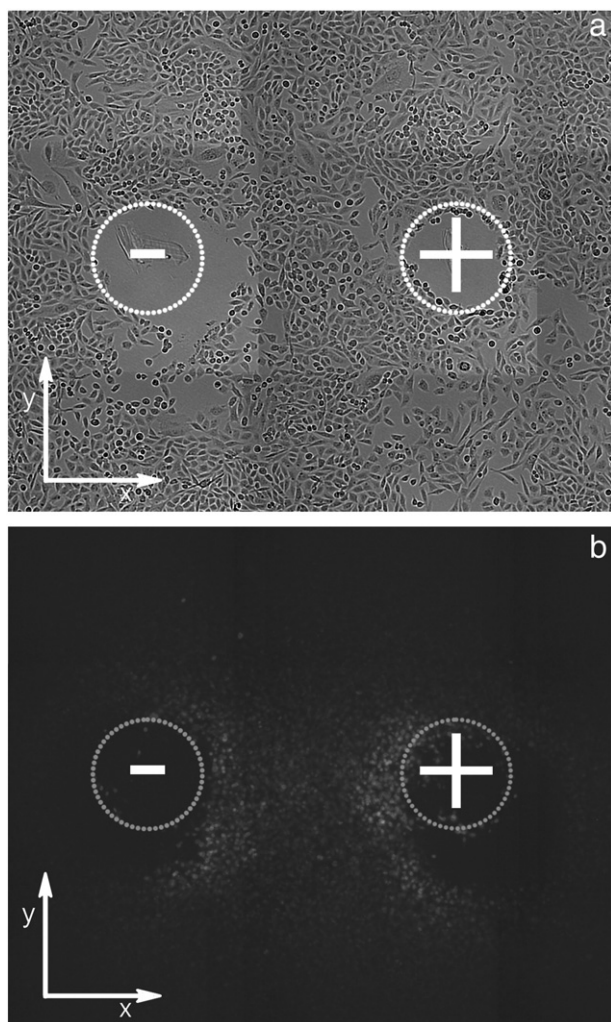


**Fig. 3.** a—Phase contrast composed image from under the microscope, 10× magnification, approximate position of the electrodes is marked with + and – signs. b—Composed fluorescent image from under the microscope, 10× magnification, averaged 6 images, applied one pulse of 120 V, approximate position of the electrodes is marked with white circles, polarity of the electrodes is marked with + and – signs.

the whole analyzed area without the electrodes taken by each of the ranges of electric field when different voltages are applied. Up to 0.8 kV/cm the limits are the same for all the applied voltages. The closer we get to the electrodes, the faster the electric field is increasing. Limits of electric field values in the inhomogeneous field were based on the

size of the area between two contours. The upper and lower limits of the area were set so that the areas between two contours were approximately the same in size. Therefore, the limits of the areas are not the same for different voltages applied (Table 3). For each of the applied voltages the corresponding contours (limits of the ranges of electric field) were superimposed to the microscopic images. An example of contours superimposed to the fluorescent image can be seen in Fig. 5c. The maximal values from Table 3 are based on a numerical calculation where this was the highest electric field value achieved when corresponding voltage was applied.

For each subarea from Table 3 cells on phase contrast images and on thresholded fluorescent images (Fig. 6a) were manually counted. The percentage of the electroporation and standard deviation in each area were determined.

In Comsol we transformed the calculated inhomogeneous electric field into the predicted percentage of the electroporated cells in the dependence on the geometry (Fig. 6b). We achieved transformation by using the numerically calculated inhomogeneous electric field values (Fig. 5a) in mathematical models (Eqs. (1)–(4)) with optimized coefficients to determine the predicted percentage of electroporated cells.

From the continuous distribution of the expected percentage of the electroporated cells (Fig. 6b) we determined areas with ranges of predicted percentage of electroporated cells. These areas had the same size and shape as the subareas of electric field around the electrodes (Fig. 5b). The values of the borders of these subareas were determined empirically. We put the image of areas with ranges of predicted percentage of electroporation on top of the image with areas with ranges of the electric field. We determined at which values of the borders the overlapping was complete. This allowed us to compare the predicted percentage of electroporation and the experimentally determined percentage of electroporation in the same subarea. The comparison was made for each of the mathematical models (Eqs. (1)–(4)) with optimized coefficients.

### 3. Results

We first determined the percentage of the electroporated cells exposed to a homogeneous electric field, and determined the influence of the cell density by fitting different mathematical models to the experimental data. Then we used the model with the best fit (highest  $R^2$ ) to predict cell electroporation in the inhomogeneous field. Predicted values were compared to experimentally determined cell permeabilization in the inhomogeneous field.

#### 3.1. Cell electroporation in a homogeneous electric field

Each of the four proposed mathematical models of electroporation (Eqs. (1)–(4)) was fitted to the experimental data from all three cell density groups, i.e. less than 300 cells per image, 300 to 600 cells per

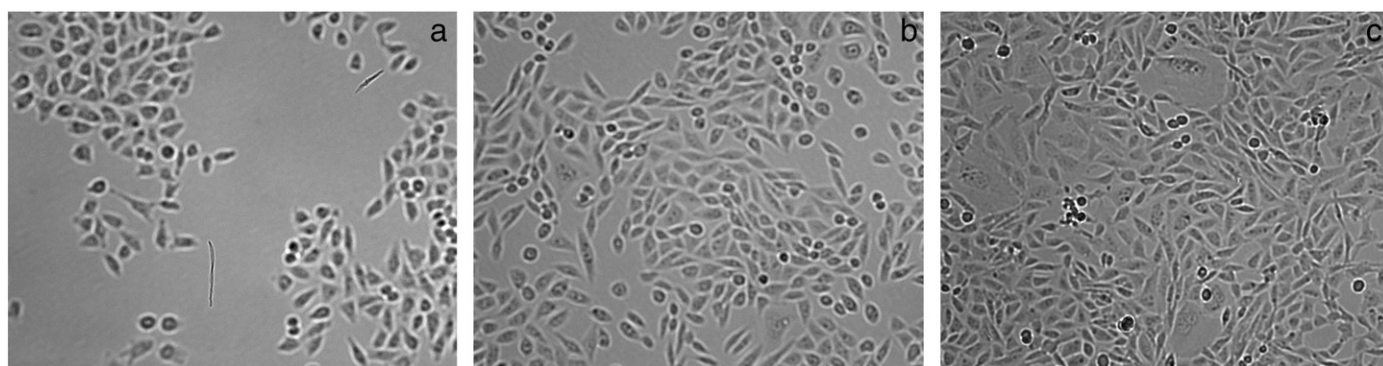


**Fig. 4.** Phase contrast microscopic images with different numbers of cells. a—Image belongs to the density group of under 300 cells per image. b—Image belongs to the density group of 300 to 600 cells per image. c—Image belongs to the density group of more than 600 cells per image.

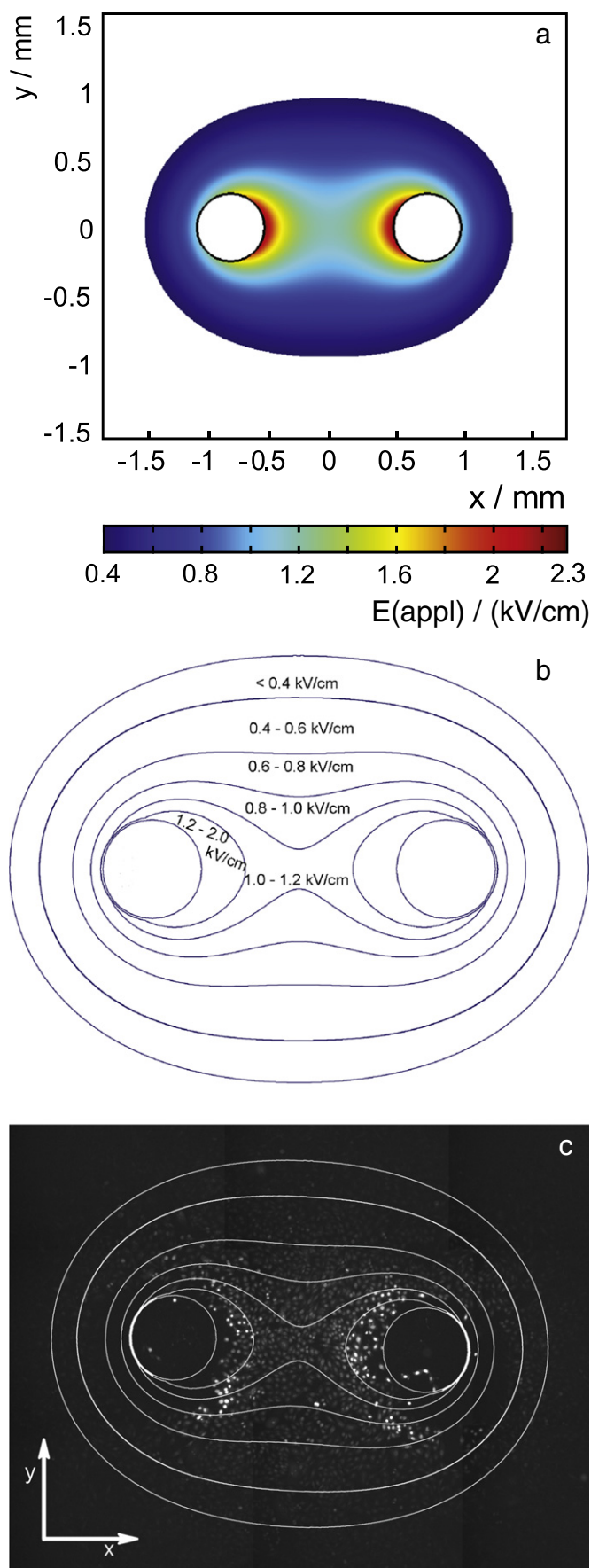


image and more than 600 cells per image.  $R^2$  value and optimized parameters for all four mathematical models (Eqs. (1)–(2)) and all three density groups can be seen in Table 4.  $R^2$  measures how successful the fit is in explaining the variation of the data i.e.  $R^2$  is the correlation between predicted and observed values. The parameter  $R^2$  was 0.990 or higher in all fits. Based on the experimental data which can be seen in Fig. 7 (triangles) we can see that the percentage of electroporated cells depends significantly on the cell density. In Fig. 7 data is presented only with Gompertz curve—the reason is explained later in this section. Somewhat surprising, the mathematical models of electroporation are not shifting to the higher values of  $E$  but are changing their slopes with different densities of the monolayer. All of the curves start to increase at approximately the same point (0.4 kV/cm) but reach their plateaus at different values of the electric field (1.2 kV/cm or more). At lower values of the electric field (less than 0.4 kV/cm) there was no electroporation detected. At the middle values of the electric field (0.4 kV/cm–1.2 kV/cm) where the curves are approximately linear, the slopes of the fitted models are different for each of the ranges of densities. When the density of the cells was lower the curve was steeper. We can see the change in the slope in Fig. 7 where the Gompertz curve (Eq. (3)) was fitted to all three density groups.

For further analysis images with the density of the cells in the range from 300 to 600 cells per image were chosen. In the experiments in the inhomogeneous electric field the actual density of the cells was higher in some areas of the composed image (more than 600 cells per image) but lower in the others. Therefore, 300 to 600 cells per image were selected as an approximation for an average cell density and further analysis was based only on density from 300 to 600 cells per image.

Fig. 8 presents the influence of the chosen mathematical model on the predicted percentage of electroporated cells. It seems as if there were only two different models shown instead of four. Namely, hyperbolic tangent and symmetric sigmoid are completely overlapping and therefore there is no visible difference on the graph. The same is true for the Gompertz curve and asymmetric sigmoid. All the mathematical models were used with parameters fitted to data from experiments in the homogeneous field. From the  $R^2$  coefficients in Table 4 we can observe that the Gompertz curve and asymmetric sigmoid when the density of the cells is 300–600 cells per image offer the best fit to the experimental data of the four curves used. Although Gompertz curve and asymmetric sigmoid are overlapping and both offer almost equally good fit to the experimental data we have chosen the Gompertz curve (Eq. (3)) for further analysis.

In Fig. 7 we can observe the influence of the density of the monolayer, whereas in Fig. 8 we can see the influence of the chosen mathematical model on the percentage of electroporation. Fig. 9 is based on Figs. 7 and 8, as it combines the appropriate density of the monolayer (Fig. 7) and the best fit based on the  $R^2$  value (Fig. 8). The appropriate density is the density of the monolayer exposed to an inhomogeneous field, i.e. 300–600 cells per image.

### 3.2. Cell electroporation in an inhomogeneous electric field

On the basis of the results acquired in experiments in the homogeneous electric field and the model of geometry of the two needle electrodes different mathematical models of cell electroporation as a function of electric field (Eqs. (1)–(4)) were applied to the numerically calculated inhomogeneous electric field.

We transformed a numerically calculated electric field (Fig. 5a) into the predicted percentage of the electroporated cells (Fig. 6b). In Fig. 9

**Fig. 5.** Distribution of the electric field strength in the plane of cell monolayer. a—Continuous distribution of the electric field strength when 120 V is applied. b—Contours which mark the borders between different ranges of the electric field when 120 V is applied. Range of electric field in a certain area is written in the corresponding area. c—Fluorescent microscopic composed image with superimposed contours of ranges of electric field, one 1 ms pulse of 120 V applied.

**Table 3**

Ranges of E-field vector when different voltages are applied and the size of the area in percents of the whole analyzed area without the electrodes. If a certain range is not analyzed when that voltage is applied there is a sign – in the corresponding cell. When the sum of percentages is not 100% it is so because of rounding of the numbers.

E-field strength range (kV/cm)	80 V area (%)	100 V area (%)	120 V area (%)	140 V area (%)
0.3–0.4	33	30	29	28
0.4–0.6	47	33	29	28
0.6–0.8	12	19	16	15
0.8–1.0	–	12	13	10
0.8–1.5	8	–	–	–
1.0–1.2	–	–	7	10
1.0–1.6	–	6	–	–
1.2–2.0	–	–	5	–
1.2–2.3	–	–	–	9

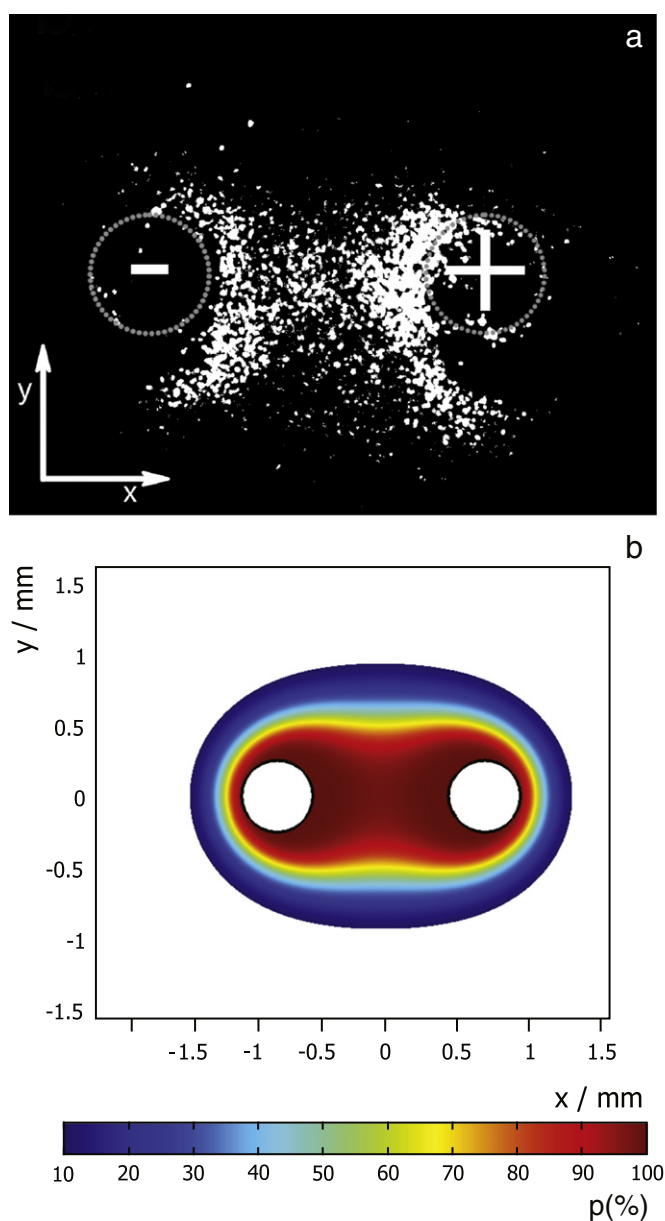


**Fig. 6.** a—Thresholded fluorescent microscopic image, averaged 6 images, approximate position of the electrodes is marked with gray circles; signs + and – in the circles mark the polarity of the electrodes. b—Predicted percentage of the electroporated cells ( $p$ ) in the plane of cell monolayer when 120 V is applied; transformation from the electric field strength to the predicted percentage is made by the Gompertz curve for densities from 300 to 600 cells per image.

we can see both the theoretically predicted and experimentally determined values. With the variation of the different models used for modeling the phenomena the difference in predicted ranges was minimal. This can be seen from comparing black vertical bars (Gompertz curve (Eq. (3)), 300 to 600 cells per image) and dark gray vertical bars (symmetric sigmoid (Eq. (1)), 300 to 600 cells per image) in Fig. 9. The predicted ranges of the percentage of the electroporated cells are almost the same. The difference in ranges was maximally 4% at lower electric field strengths. If we compare ranges predicted by these two curves (Eqs. (1) and (3)) based on the same density (300 to 600 cells per image) with the light gray bars, which represent a denser monolayer (more than 600 cells per image), we can observe that the predicted ranges are quite different at lower as well as at higher electric field strengths. Other combinations of the interpolation curve and the density of the cells were made as well (Table 4) but for the sake of stressing the influence of the density and of the mathematical model only the Gompertz curve for 300–600 and more than 600 cells per image and symmetric sigmoid for 300–600 cells per image are shown. Aside from the symmetric sigmoid (Eq. (1)) also the hyperbolic tangent (Eq. (4)) could be shown.

#### 4. Discussion

The aim of our study was to compare different mathematical models that would allow transformation of the numerically calculated values of the electric field into the predicted percentage of electroporated cells. This kind of transformation and prediction would simplify presentation of treatment plans for electrochemotherapy and non-thermal irreversible electroporation. We upgraded the usual assumption that the percentage of the electroporated cells is 100% if the electric field is above the characteristic threshold and 0% if it is below [49]. Here the prediction was continuous and all the values between 0% and 100% were predicted. We investigated and compared the effects of the cell density and of the used mathematical model (Eqs. (1)–(4)). We started our study with the model of continuous electric field distribution presented in Fig. 5a, transforming it into the predicted percentage of electroporated cells as shown in Fig. 6b. In Fig. 6a we can see that the pattern of the electroporated and non-electroporated cells is in good agreement with the predicted shape in Fig. 6b.

If we look at Fig. 6a it appears as if there were more cells electroporated around the positive electrode. However, the analysis of the percentages of electroporated cells around each of the electrode (data not shown) showed that there was no significant difference between the percentages around the positive and around the negative electrode.

In the course of the transformation from the electric field strength in the homogeneous field to the percentage of electroporated cells in the inhomogeneous electric field we reached two main conclusions. The first one was about the changing of the slope of the mathematical model of electroporation in the homogeneous field and the second one was about the choice of the mathematical model, fitted to the

**Table 4**  
Results for the goodness of the fit ( $R^2$ ) and the curves' parameters for all of the four proposed curves for all three density groups. The fit is based on the percentage of electroperated cells in the homogenous field. The parameters are explained in 2.4 Fitting of the mathematical models.

Type of the curve	R-square <sup>a</sup>			Parameters		
	<300 cells/image	300–600 cells/image	>600 cells/image	<300 cells/image	300–600 cells/image	>600 cells/image
Symmetric sigmoid	0.992	0.990	0.964	$E_{50\%} = 0.659$ $b = 0.1090$	$E_{50\%} = 0.6879$ $b = 0.1242$	$E_{50\%} = 0.9231$ $b = 0.2353$
Asymmetric sigmoid	0.997	0.998	0.965	$E_{50\%} = 0.5869$ $v = 5e-8$ (fixed at bound) $b = 0.1529$	$E_{50\%} = 0.6061$ $v = 2e-8$ (fixed at bound) $b = 0.1772$	$E_{50\%} = 1.057$ $v = 2.557$ $b = 0.1494$
Gompertz curve	0.997	0.998	0.958	$E_{50\%} = 0.5869$ $b = 0.1529$	$E_{50\%} = 0.6061$ $b = 0.1772$	$E_{50\%} = 0.7567$ $b = 0.343$
Hyperbolic tangent	0.992	0.990	0.964	$E_{50\%} = 0.659$ $B = 4.587$	$E_{50\%} = 0.6879$ $B = 4.027$	$E_{50\%} = 0.9231$ $B = 0.9231$

<sup>a</sup> Goodness-of-fit.

experimental data. In general results obtained are in good agreement with the results found in the literature, describing experiments with suspensions. Nevertheless, the change of the models' slopes with respect to cell density seems rather surprising and contradictory to theoretical considerations [47].

First, we will discuss the change of models' slope. Experimental observation where the slope of the model changes can be observed in [35]. There we can see that the curve of detected fluorescence shifted with a change of pulse parameters (when longer pulses were used the slope was steeper). No curve which would show the dependence on the cell density is shown; we can only see that with the same pulse protocol and higher density of the suspension fewer cells are electroperated.

As it can be observed from Fig. 7, the model of electroperation did not shift but changed its slope when monolayers of cells with different densities were used for experiments. In previous studies it has been observed that with increasing densities of cell suspensions the base point of the curves and the point where the curves reach their plateaus shifted to the higher electric field with the slope of the curve being the same [47]. In our study one part of the observation was similar—the points where the curves reach their plateau values shifted to the higher electric field values when we increased the density of the cell monolayer. On the other hand, the base point where a minimal fluorescence of the cells

was detected was the same for all of the densities. Therefore, the slope of the curves changed.

It is known that with denser suspensions we get lower induced transmembrane voltage due to the mutual electrical shielding [33–36]. In the monolayers the situation is the same—with denser monolayers we get lower induced transmembrane voltage and lower percentage of the electroperated cells. However, we should not neglect the effect of the cells' geometry [50,51] which is deviatory from spheres and the electrical connections between the cells, e.g. gap junctions [52]. It seems that the cell's geometry and connections between the cells are related to the curves' slopes, which might be an area of further research.

The standard deviation in Figs. 7 and 8 is relatively high; the reason is counting of the cells. All means of cell counting are subjected to errors because of noise and artifacts, various cell shapes, and cells in close contact without clear boundaries between them. Considering that we had monolayers of very high density the calculated standard deviation is within the expected values as reported in the literature [53]. The error would be lower if using cells in suspension; however the cells in suspension and in tissues behave very differently. In a suspension there are no connections between the cells and they are all approximately spherical.

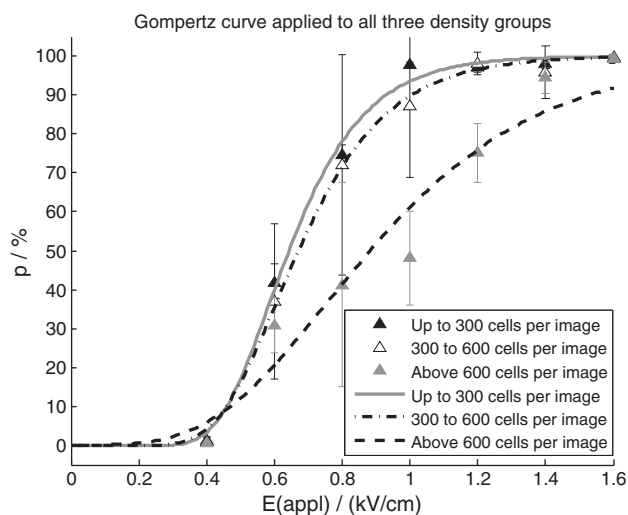


**Fig. 7.** Percentage ( $p$ ) of electroperated cells determined by propidium iodide staining in the dependence on the applied electric field. The Gompertz curve is fitted to all three groups of different densities of the cells. Mean experimental values from experiments, made in the homogeneous field are marked with triangles; vertical bar denotes one standard deviation. Black triangle and gray solid line represent density up to 300 cells per image, hollow triangle and dotted black line represent density from 300 to 600 cells per image, and gray triangle and dashed black line represent density above 600 cells per image.

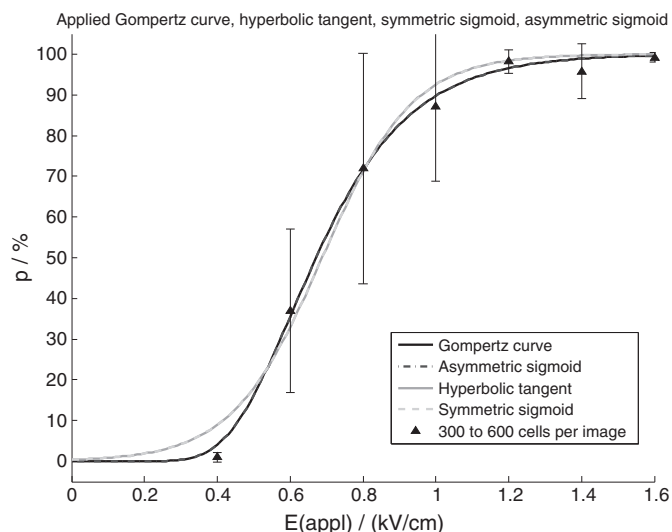


**Fig. 8.** Percentage ( $p$ ) of electroperated cells determined by propidium iodide staining in dependence on the applied electric field. Four different models of electroperation were fitted to the experimental data of the percentage of electroperated cells in the homogeneous field. Triangles represent the mean experimental values for the percentage of electroperated cells in the homogeneous electric field; vertical bar denotes one standard deviation. Black solid line represents Gompertz line, black dashed line represents asymmetric sigmoid, gray solid line represents hyperbolic tangent and gray dashed line represents symmetric sigmoid.

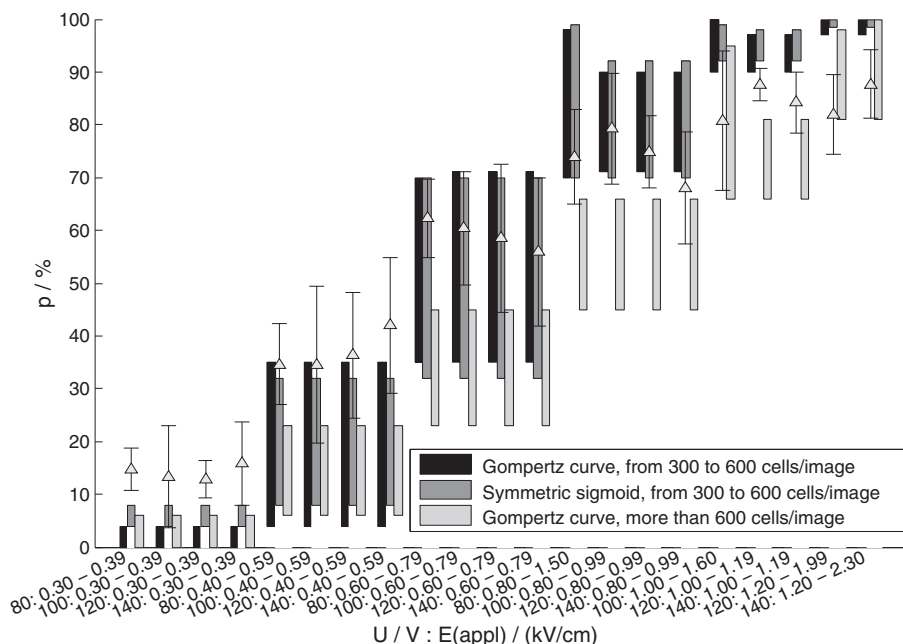


**Fig. 9.** Predicted (vertical bars) and experimentally determined percentage (triangles) of the electroporation; model for a cell response made by the Gompertz curve (Eq. (3)) and symmetric sigmoid (Eq. (1)) for different densities. Three bars in one set from left to right are the Gompertz curve for densities from 300 to 600 cells per image (black bar), the symmetric sigmoid for densities from 300 to 600 cells per image (dark gray bar) and the last bar the Gompertz curve for densities of more than 600 cells per image (light gray bar). The vertical bar at experimentally determined values represents one standard deviation. Labels on the x-axis mean the applied voltage and the area with the corresponding electric field range for that applied voltage.

In the past, different mathematical models have been proposed for describing the dependence between the percentage of the electroporated cells and the electric field. For example, a hyperbolic tangent law for permeabilization as a function of the electric field has been proposed [47]. In statistical physics the hyperbolic tangent is commonly used for describing two-state systems, for example the polarized light. Similarly, electroporated and non-electroporated cells can also be viewed as two states in a system and hyperbolic tangent law describes the crossover from the non-electroporated to the electroporated state.

In [20] two different ways of describing the cell electroporation fraction have been used. The first one was sigmoid function which is often fitted to the experimental data. The second one was a curve which derived from a hypothetical normal distribution of cell radii. In this case the curve was obtained from a step function (electroporation is 0% when the applied electric field is under the threshold for electroporation and 100% when the applied electric field is above the threshold). Cell radius was varied according to the normal distribution with empirically determined values for mean cell radius and its standard deviation. Goodness-of-fit between the normal distribution curve on one side and the experiments on the other showed that experimental results were in good agreement with the theoretically predicted values. Nevertheless, the authors could not decide which of the two curves was more appropriate.

The Gompertz curve is used for describing the systems which saturate in a long period of time, for example the growth of the tumors [46]. The growth is slower at the beginning. Then the size starts to increase faster. The growth is limited after a certain time period when the size of the tumor reaches a plateau value. The growth can be compared to the percentage of cell electroporation as a function of the electric field where we obtain high percentage of cells being electroporated, but with an increasing electric field the increase e.g. from 97% to 100% of electroporated cells is difficult to obtain.

Up to a certain electric field reached there are almost no cells electroporated. From 0.4 kV/cm to 1.0 kV/cm the percentage of the electroporated cells quickly increases and then it reaches the plateau value. The described logic is the reason that we proposed the Gompertz curve for describing the electroporation of the cells. It is not necessary

that the Gompertz curve is symmetric. The asymmetry in the model is appropriate because in reality the percentage of the electroporated cells depends also on the cell radius, and according to the literature the cell radii are not symmetrically distributed [20] which was also the case in our study (data not shown).

Therefore, we can expect that the mathematical model of electroporation is asymmetric as well. This asymmetry was also the reason why we chose the asymmetric sigmoid curve for analysis.

So far not many studies of a statistical evaluation of electroporation are available. For evaluating the area of irreversible electroporation a statistical model based on the Peleg–Fermi model combined with a numerical solution of the multidimensional electric field equation cast in a dimensionless form was used [21]. This model directly incorporates the dependence of cell death on pulse number ( $n$ ) and on electric field ( $E$ ). It is expressed by Eqs. (5)–(7), where  $S$  means the survival ratio and  $E_c$  marks the intersection of the curve with the y-axis. Coefficients  $k_1$  and  $k_2$  are cell type and pulse type specific.

$$S = 1 / (1 + \exp(E - E_c(n)) / A(n)) \tag{5}$$

$$E_c(n) = E_{c0} * \exp(-k_1 * n) \tag{6}$$

$$A(n) = A_0 * \exp(-k_2 * n) \tag{7}$$

The problem with this model is that it was not validated since it was tested only on extrapolated data reported in the literature for prostate cancer cell death caused by irreversible electroporation [54]. Authors stated that real curves and parameters should be developed for each specific tissue. Also the Fermi–Peleg model should be validated first in vitro and then in vivo.

Several microbial inactivation curves have been effectively described by Weibull distribution. In this model parameters were dependent on the media type and treatment parameters (electric field and treatment time) [22,55] but not on pulse number and pulse length like the Peleg–Fermi statistical model. Therefore, this model is not as interesting

for our study as the Peleg–Fermi model. Also, in the area of microbial inactivation by pulsed electric fields many mathematical models exist [22, 56], but they all describe survival of the cells in dependence on applied electric field and treatment time, with treatment time most often reported as the sum of duration of all of the applied pulses. All these models (Weibull, Peleg–Fermi, log-linear etc.) describe the survival of the cells. In our study on the other hand, survival of the cells has not been determined. Therefore, these models were not used in our study.

In our study four mathematical models (Eqs. (1)–(4)) were chosen, used and evaluated. We achieved good agreement with all of them since  $R^2$  was 0.990 or higher in all four cases (see Table 4); therefore, for the analysis of the effect of the cell density on electroporation any of them might be used. For further analysis of the effect of cell density we considered the two curves with the highest  $R^2$ —Gompertz curve and asymmetric sigmoid. If parameter  $\nu$  in the asymmetric sigmoid model (Eq. (2)) was negative, no fit could be achieved because complex values were computed by model function. Therefore, we set a lower limit for this parameter at 0. Although we managed to complete the fitting, the parameter  $\nu$  was fixed at bound, which meant that the best fit was not achieved. The asymmetric sigmoid model was thus not used in the next step of the analysis.

For the analysis of the effect of the interpolation curve on the prediction of the percentage of electroporation we used only the Gompertz curve (Eq. (3)) and symmetric sigmoid (Eq. (1)). There was no need to do the analysis both with hyperbolic tangent (Eq. (4)) and symmetric sigmoid (Eq. (1)) since they can be seen as equivalent (see their overlapping in Fig. 8).

If we look at Fig. 9 we can see that under our experimental conditions the percentage of the affected cells depends more on the density of the cells than on a type of the curve. When different curve was used for the same density (compare dark gray bars for the symmetric sigmoid (Eq. (1)) and black bars for the Gompertz curve (Eq. (3)) in Fig. 9) the difference between predicted ranges was 4% at lower electric field strengths (0.30–0.39 kV/cm) and even less for the higher ones. The reason for the 4% difference can be observed from Fig. 8. There we can see that at lower electric field values Eqs. (1) and (3) deviate the most one from another.

At lower electric field values the symmetric sigmoid overestimates the experimental results while the Gompertz curve offers better fit. This means that the percentage predicted by the symmetric sigmoid (Eq. (1)) is higher than the one predicted by the Gompertz curve (Eq. (3)) which is not in very good agreement with experimental results. But since the predicted ranges of electroporation are still quite similar (0–4% for Eq. (3) and 4–8% for Eq. (1)) and they both underestimate experimental results we can conclude that the choice of the curve is not of highest importance.

The reason for discrepancy at the higher electric field could be the fact that mathematical models for electroporation allow 100% electroporation although in reality there are always some cells which do not respond to electric pulses and stay unaffected at least to very high values of electric field. This is particularly true with single pulse applied at very high electric fields (data not shown) as was the case in our experiments. This could be the reason why the predicted ranges in Fig. 9 are above the experimentally measured values.

In vitro a small fraction of dead cells is always detected, which explains the deviation of experimental data at the lowest electric field strength from theoretical prediction by mathematical models for electroporation.

If we look at the light gray bars at Fig. 9 (Gompertz curve (Eq. (3)) for densities above 600 cells) per image, we can see that they do not reproduce the experimental results (triangles) properly. The mathematical model of electroporation is underestimating the experimental results at all of the applied electric field strengths for at least 10%. The reason is in the density of the cells. Prediction was made on monolayers of more than 600 cells per image. The experiments were performed

on monolayers of less than 600 cells per image. This means that the density of the cells is a very important factor. It must be the same in experiments used for prediction and in experiments where we predict the percentage of electroporated cells. The prediction offered better agreement only at the higher values of the electric field because the electric field was already strong enough for all of the curves to reach their plateau values. Therefore, we can say that the density of the cell monolayer is very important for predicting the percentage of electroporation.

In previously published works a strong dependence between the cells' electroporation and the density of the cells was already shown [33,34]. In our study we went one step further and showed that the cell density not only has a strong influence on the cells' electroporation but is under our experimental conditions the most important factor influencing the prediction of electroporation. We eliminated the effect of the size of the cells since the experiments in homogeneous and inhomogeneous field were made on monolayers of similar density. Our experiments have been performed in vitro on CHO cells. Our results were obtained using single pulse of 1 ms duration; however we need to establish how the parameters of curves depend on duration and number of pulses, and different cells. In addition, there might be other parameters besides the density of the cells which have an important influence on the prediction of electroporation. How this translates into tissue remains to be determined; tissue level determination and validation are still needed [38,39].

## Acknowledgments

This study was supported by the Slovenian Research Agency (ARRS) and conducted within the scope of the Electroporation in Biology and Medicine European Associated Laboratory (LEA-EBAM). Authors (J.D.) would like to acknowledge doc. dr. Gorazd Pucihar and Duša Hodžič for their guidance when starting to work in cell laboratory. Experimental work was performed in the infrastructure center 'Cellular Electrical Engineering'.

## References

- [1] E. Neumann, K. Rosenheck, Permeability changes induced by electric impulses in vesicular membranes, *J. Membr. Biol.* 10 (1972) 279–290.
- [2] T. Kotnik, P. Kramar, G. Pucihar, D. Miklavčič, M. Tarek, Cell membrane electroporation—Part 1: the phenomenon, *Electr. Insul. Mag.* 28 (2012) 14–23.
- [3] T.Y. Tsong, Electroporation of cell membranes, *Biophys. J.* 60 (1991) 297–306.
- [4] T. Kotnik, G. Pucihar, D. Miklavčič, Induced transmembrane voltage and its correlation with electroporation-mediated molecular transport, *J. Membr. Biol.* 236 (2010) 3–13.
- [5] M. Čemažar, T. Jarm, D. Miklavčič, A. Maček Lebar, A. Ihan, N.A. Kopitar, et al., Effect of electric-field intensity on electroporation and electrosensitivity of various tumor-cell lines in vitro, *Electro-Magnetobiol.* 17 (1998) 263–272.
- [6] B. Rubinsky, G. Onik, P. Mikus, Irreversible electroporation: a new ablation modality—clinical implications, *Technol. Cancer Res. Treat.* 6 (2007).
- [7] E. Neumann, M. Schaefer-Ridder, Y. Wang, P.H. Hofschneider, Gene transfer into mouse lymphoma cells by electroporation in high electric fields, *EMBO J.* 1 (1982) 841–845.
- [8] L.C. Heller, R. Heller, Electroporation gene therapy preclinical and clinical trials for melanoma, *Curr. Gene Ther.* 10 (2010) 312–317.
- [9] A.I. Daud, R.C. DeConti, S. Andrews, P. Urbas, A.I. Riker, V.K. Sondak, et al., Phase I trial of interleukin-12 plasmid electroporation in patients with metastatic melanoma, *J. Clin. Oncol.* 26 (2008) 5896–5903.
- [10] L.M. Mir, Therapeutic perspectives of in vivo cell electroporation, *Bioelectrochemistry* 53 (2001) 1–10.
- [11] B. Mali, T. Jarm, M. Snoj, G. Serša, D. Miklavčič, Antitumor effectiveness of electrochemo-therapy: a systematic review and meta-analysis, *Eur. J. Surg. Oncol.* 39 (2013) 4–16.
- [12] D. Miklavčič, G. Serša, E. Brecelj, J. Gehl, D. Soden, G. Bianchi, et al., Electrochemotherapy: technological advancements for efficient electroporation-based treatment of internal tumors, *Med. Biol. Eng. Comput.* 50 (2012) 1213–1225.
- [13] J. Teissié, N. Eynard, M.-C. Vernhes, A. Bénichou, V. Ganeva, B. Galutzov, et al., Recent biotechnological developments of electroporation. A prospective review, *Bioelectrochemistry* 55 (2002) 107–112.
- [14] S. Haberl, M. Jarc, A. Štrancar, M. Peterka, D. Hodžič, D. Miklavčič, Comparison of alkaline lysis with electroextraction and optimization of electric pulses to extract plasmid DNA from *Escherichia coli*, *J. Membr. Biol.* 246 (11) (2013) 861–867.

- [15] H.L.M. Lelievre, S. Notermans, S.W.H. de Haan, *Food Preservation by Pulsed Electric Fields: From Research to Application*, World Publishing Limited, Cambridge, England, 2007.
- [16] S. Schilling, S. Schmid, H. Jaeger, M. Ludwig, H. Dietrich, S. Toepfl, et al., Comparative study of pulsed electric field and thermal processing of apple juice with particular consideration of juice quality and enzyme deactivation, *J. Agric. Food Chem.* 56 (2008) 4545–4554.
- [17] S. Haberl, D. Miklavčič, G. Serša, W. Frey, B. Rubinsky, Cell membrane electroporation—Part 2: the applications, *IEEE Electr. Insul. Mag.* 29 (2013) 29–37.
- [18] E. Tekle, R.D. Astumian, P.B. Chock, Electro-permeabilization of cell membranes: effect of the resting membrane potential, *Biochem. Biophys. Res. Commun.* 172 (1990) 282–287.
- [19] J. Teissié, M.-P. Rols, An experimental evaluation of the critical potential difference inducing cell membrane electroporation, *Biophys. J.* 65 (1993) 409–413.
- [20] M. Puc, T. Kotnik, L.M. Mir, D. Miklavčič, Quantitative model of small molecules uptake after in vitro cell electroporation, *Bioelectrochemistry* 60 (2003) 1–10.
- [21] A. Goldberg, B. Rubinsky, A statistical model for multidimensional irreversible electroporation cell death in tissue, *Biomed. Eng. OnLine* 9 (2010).
- [22] M.F. San Martín, D.R. Sepúlveda, B. Altunakar, M.M. Góngora-Nieto, B.G. Swanson, G. V. Barbosa-Cánovas, Evaluation of selected mathematical models to predict the inactivation of *Listeria innocua* by pulsed electric fields, *LWT* 40 (2007) 1271–1279.
- [23] B. Mali, D. Miklavčič, L.G. Campana, M. Čemažar, G. Serša, M. Snoj, et al., Tumor size and effectiveness of electrochemotherapy, *Radiol. Oncol.* 47 (2013) 32–41.
- [24] I. Edhemovic, E.M. Gadzijevec, E. Brečelj, D. Miklavčič, B. Kos, A. Županič, et al., Electrochemotherapy: a new technological approach in treatment of metastases in the liver, *Technol. Cancer Res. Treat.* 10 (2011) 475–485.
- [25] F. Mahmood, J. Gehl, Optimizing clinical performance and geometrical robustness of a new electrode device for intracranial tumor electroporation, *Bioelectrochemistry* 81 (2011) 10–16.
- [26] R.E. Neal, J.H. Rossmeisl, P.A. Garcia, O.I. Lanz, N. Henao-Guerrero, R.V. Davalos, Successful treatment of a large soft tissue sarcoma with irreversible electroporation, *J. Clin. Oncol.* 29 (2011) e372–e377.
- [27] G. Onik, B. Rubinsky, Irreversible electroporation: first patient experience focal therapy of prostate cancer, in: B. Rubinsky (Ed.), *Irreversible Electroporation*, Springer Berlin Heidelberg, Berlin, Heidelberg, 2010, pp. 235–247.
- [28] D. Miklavcic, M. Snoj, A. Županic, B. Kos, M. Cemazar, M. Kropivnik, et al., Towards treatment planning and treatment of deep-seated solid tumors by electrochemotherapy, *Biomed. Eng. OnLine* 9 (2010) 10.
- [29] D. Pavliha, B. Kos, A. Županič, M. Marčan, G. Serša, D. Miklavčič, Patient-specific treatment planning of electrochemotherapy: procedure design and possible pitfalls, *Bioelectrochemistry* 87 (2012) 265–273.
- [30] P.A. Garcia, J.H. Rossmeisl, R.E. Neal, T.L. Ellis, R.V. Davalos, A parametric study delineating irreversible electroporation from thermal damage based on a minimally invasive intracranial procedure, *Biomed. Eng. OnLine* 10 (2011) 34.
- [31] A. Županič, B. Kos, D. Miklavčič, Treatment planning of electroporation-based medical interventions: electrochemotherapy, gene electrotransfer and irreversible electroporation, *Phys. Med. Biol.* 57 (2012) 5425–5440.
- [32] A. Županič, D. Miklavčič, Tissue heating during tumor ablation with irreversible electroporation, *Elektroteh. Vestn.* 78 (2011) 42–47.
- [33] M. Pavlin, N. Pavšelj, D. Miklavčič, Dependence of induced transmembrane potential on cell density, arrangement, and cell position inside a cell system, *IEEE Trans. Biomed. Eng.* 49 (2002) 605–612.
- [34] R. Susil, D. Šemrov, D. Miklavčič, Electric field induced transmembrane potential depends on cell density and organization, *Electro- Magnetobiol.* 17 (1998) 391–399.
- [35] G. Pucihar, T. Kotnik, J. Teissié, D. Miklavčič, Electroporation of dense cell suspensions, *Eur. Biophys. J.* 36 (2007) 172–185.
- [36] M. Pavlin, D. Miklavčič, The effective conductivity and the induced transmembrane potential in dense cell systems exposed to DC and AC electric fields, *IEEE Trans. Plasma Sci.* 37 (2009).
- [37] D. Miklavčič, D. Šemrov, H. Mekid, L.M. Mir, A validated model of in vivo electric field distribution in tissues for electrochemotherapy and for DNA electrotransfer for gene therapy, *Biochim. Biophys. Acta* 1523 (2000) 73–83.
- [38] Z. Qin, J. Jiang, G. Long, B. Lindgren, J.C. Bischof, Irreversible electroporation: an in vivo study with dorsal skin fold chamber, *Ann. Biomed. Eng.* 41 (2013) 619–629.
- [39] R.E. Neal, J.L. Millar, H. Kavnoudias, P. Royce, F. Rosenfeldt, A. Pham, et al., In vivo characterization and numerical simulation of prostate properties for non-thermal irreversible electroporation ablation: characterized and simulated prostate IRE, *Prostate* 74 (5) (2014) 458–468.
- [40] N. Pavšelj, D. Miklavčič, Numerical modeling in electroporation-based biomedical applications, *Radiol. Oncol.* 42 (2008) 159–168.
- [41] M. Kranjc, F. Bajd, I. Sersa, D. Miklavcic, Magnetic resonance electrical impedance tomography for monitoring electric field distribution during tissue electroporation, *IEEE Trans. Med. Imaging* 30 (2011) 1771–1778.
- [42] M. Kranjc, F. Bajd, I. Sersa, E.J. Woo, D. Miklavcic, Ex vivo and in silico feasibility study of monitoring electric field distribution in tissue during electroporation based treatments, *PLoS One* 7 (2012) e45737.
- [43] G. Pucihar, J. Krmelj, M. Reberšek, T. Napotnik, D. Miklavčič, Equivalent pulse parameters for electroporation, *IEEE Trans. Biomed. Eng.* 58 (2011) 3279–3288.
- [44] S. Mazères, D. Šel, M. Golzio, G. Pucihar, Y. Tamzali, D. Miklavčič, et al., Non invasive contact electrodes for in vivo localized cutaneous electroporation and associated drug and nucleic acid delivery, *J. Controlled Release* (2009) 125–131.
- [45] M. Golzio, J. Teissié, Direct assay of electroporation in a 2D pseudo tissue, *Phys. Chem. Chem. Phys.* 12 (2010) 14670.
- [46] A.K. Laird, Dynamics of tumour growth, *Br. J. Cancer* 18 (1964) 490–502.
- [47] M. Essone Mezeme, G. Pucihar, M. Pavlin, C. Brosseau, D. Miklavčič, A numerical analysis of multicellular environment for modeling tissue electroporation, *Appl. Phys. Lett.* 100 (2012) 143701.
- [48] C. Polk, E. Postow, *Handbook of Biological Effects of Electromagnetic Fields*, 2nd ed. CRC Press, Florida, 2000.
- [49] B. Kos, A. Županič, T. Kotnik, M. Snoj, G. Serša, D. Miklavčič, Robustness of treatment planning for electrochemotherapy of deep-seated tumors, *J. Membr. Biol.* 236 (2010) 147–153.
- [50] L. Towhidi, T. Kotnik, G. Pucihar, S.M.P. Firoozabadi, H. Mozdarani, D. Miklavčič, Variability of the minimal transmembrane voltage resulting in detectable membrane electroporation, *Electromagn. Biol. Med.* 27 (2008) 372–385.
- [51] B. Valič, M. Golzio, M. Pavlin, A. Schatz, C. Faurie, B. Gabriel, et al., Effect of electric field induced transmembrane potential on spheroidal cells: theory and experiment, *Eur. Biophys. J.* (2003) 519–528.
- [52] G. Pucihar, D. Miklavčič, The influence of intracellular connections on the electric field induced membrane voltage and electroporation of cells in clusters, in: O. Dössel, W.C. Schlegel (Eds.), *World Congr. Med. Phys. Biomed. Eng. Sept. 7–12 2009 Munich Ger.*, Springer Berlin Heidelberg, Berlin, Heidelberg, 2009, pp. 74–77.
- [53] M. Usaj, D. Torkar, M. Kanduser, D. Miklavcic, Cell counting tool parameters optimization approach for electroporation efficiency determination of attached cells in phase contrast images: cell counting tool parameters optimization approach, *J. Microsc.* 241 (2011) 303–314.
- [54] P.J. Canatella, J.F. Karr, J.A. Petros, M.R. Prausnitz, Quantitative study of electroporation-mediated molecular uptake and cell viability, *Biophys. J.* 80 (2001) 755–764.
- [55] I. Álvarez, J. Raso, F.J. Sala, S. Condón, Inactivation of *Yersinia enterocolitica* by pulsed electric fields, *Food Microbiol.* 20 (2003) 691–700.
- [56] I. Álvarez, R. Virto, J. Raso, S. Condón, Comparing predicting models for the *Escherichia coli* inactivation by pulsed electric fields, *Innov. Food Sci. Emerg. Technol.* 4 (2003) 195–202.